One-nanometer luminous silicon nanoparticles: Possibility of a fullerene interpretation

Aristides D. Zdetsis
Department of Physics, University of Patras, 26500 GR, Patras, Greece
(Received 11 November 2008; revised manuscript received 20 January 2009; published 28 May 2009)

It is shown here by *ab initio* calculations that embedded silicon fullerenes of the form $Si@Si_{28}H_{28}$, $Si^{1-}@Si_{28}H_{28}$, and $Si_5@Si_{24}H_{24}$ could be consistent with most of the known, experimental data concerning the structural prototype of the 1 nm silicon nanostructure responsible for the ultrabright blue luminescence. It is also demonstrated that the route of formation of the common reconstructed $Si_{29}H_{24}$ nanoparticle originates from such embedded fullerenes rather than from the $Si_{29}H_{36}$ bulk nanocrystal. The structural models based on the fullerene interpretation compare favorably energetically with the reconstructed prototype and are very attractive for applications regardless of their relation or not with the ultrabright silicon nanoparticle. Observed discrepancies in the calculated excitation spectra can be reconciled by additional plausible assumptions. The emerging picture is very attractive and intriguing, suggestive of novel fundamental phenomena and technological applications in quantum computing and optoelectronics.

DOI: 10.1103/PhysRevB.79.195437 PACS number(s): 61.48.−c, 31.90.+s, 81.05.Tp, 61.46.−w

I. INTRODUCTION

The discovery of visible photoluminescence in porous silicon (p-Si) and silicon nanoparticles opened a new very active area of research, both experimentally and theoretically.[1–19] Bright silicon nanostructures are particularly intriguing in view of the poor optical properties of crystalline silicon, contrary to its excellent electronic properties. Almost ten years after the first observation of visible red luminescence by Canham[1] and almost ten years from today Nayfeh and his collaborators[16–19] obtained bright blue luminescence from isolated ultrasmall silicon nanoparticles (colloidal quantum dots) with uniform size of about 1 nm. This discovery was considered as a first significant step toward "a laser on a chip," extending the functionality of Si technology from microelectronics (and nanoelectronics) to optoelectronics and biophotonics.[19]

Following the discovery of blue luminescence from 1 nm silicon nanoparticles, the search for a structural prototype resulted[17] to a surface-reconstructed $Si_{29}H_{24}$ nanocrystal with T_d symmetry which was obtained from the bulk $Si_{29}H_{36}$ nanocrystal by elimination of 12 terminating hydrogen atoms and reconstruction (similar to the 2×1 reconstruction of the Si[001] surface of crystalline silicon). Due to its large highest occupied molecular orbital (HOMO)–lowest unoccupied molecular orbital (LUMO) (and optical) gap[5,13,19] compared to the experimental value of 3.5 eV, the bulk $Si_{29}H_{36}$ nanocrystal with an optical gap of 4.53 eV (with the TDDFT/B3LYP method, or 4.45 eV with the very accurate MR-MP2 method[5,13]) was ruled out, although, as was shown by Zdetsis and collaborators,[13–15] a partially oxygenated bulk nanocrystal of the form $Si_{29}H_{32}O_2$ or $Si_{29}H_{28}O_4$ would be also compatible with the experimental optical data.

Another possibility, and in fact another structural model which will be discussed here, arises by the recent theoretical work on silicon "fullerenes." Such fullerenes were recently suggested by Zdetsis[20,21] and others.[22–24] Zdetsis[20,21] has suggested the possibility of synthesizing (or identifying) very stable and highly symmetric cages with very large HOMO-LUMO gaps of the form Si_nH_n, $n=4-60$ similar and homologous (in particular for $n=20-60$) to the corresponding carbon "fullerenes" or "fulleranes." Almost at about the same time Kumar and Kawazoe[22,23] have considered small hydrogenated cages for $n=8-28$ in a different perspective, examining their doping with various metal atoms (doping with Zn and Ni for the $n=10$, 12 cages was also examined in detail in Ref. 20). Karttunen *et al.*[24] also at about the same time independent of this work have considered (in a different context) the stability of large icosahedral Si_nH_n "fullerenes" with $n=20$, 60, up to 540, in relation to corresponding polysilanes.

In view of the homology between analogous silicon and carbon cages illustrated recently by the present author,[21] in particular of $Si_{20}H_{20}$ and $Si_{60}H_{60}$ with $C_{20}H_{20}$ and $C_{60}H_{60}$, it is natural to consider doping the Si_nH_n cages with nonmetal atoms and ions, such as H^+, H, He, Ne, Ar, N, P, C^-, Si^-, O^+, S^+, which are very popular[25,26] for doping $C_{20}H_{20}$ (and other C_nH_n "fulleranes"). Doping with Si^- (Si^{1-}) in particular is more attractive because it leads to an all silicon (hydrogenated) structure with silicon in the center, similarly to medium and large size Si clusters (unlike C clusters).[27] Such a model is a potential candidate for the 1 nm luminous silicon-hydrogen nanoparticle, as will be shown bellow. Furthermore, endohedral fullerenes whose dopant atoms (or ions) retain (more or less) their isolated atomic states have received attention recently,[28] partly because of newly proposed solid-state quantum computers based on such materials. It is expected that the advent of such solution-processed optoelectronic materials would offer the potential for a revolution in optoelectronics since their solution processibility enables low-cost large-area monolithic integration on a variety of electronic read-out platforms.

The structural model suggested here is based on the $Si_{28}H_{28}$ fullerene. This "fullerene" has the right size and is characterized by the "right" T_d symmetry. In addition, the *embedding* or *inclusion* energy (the energy gain by inclusion of the central Si^{1-} ion) for this fullerene is the highest compared to its "neighboring" cages. This fullerene could be also important for astrophysical research, in view of the suggestion of Nayfeh *et al.*[29] that the 1 nm silicon nanoparticles are the carriers of the blue luminescence in the red rectangle nebula. This is reminiscent of (and parallel to) the suggestion

of Webster[30] about the existence of carbon fulleranes ($C_{60}H_{60}$) in interstellar space.[30,31] If the present interpretation is proven (even partially) correct by experiment, then silicon fulleranes could be found in interstellar space as well.

Alternatively, instead of doping by Si^{1-}, one could consider inclusion of a neutral Si atom, although such doping was not considered for the corresponding carbon fulleranes.[25,26] Furthermore, the energy cost is relatively high (inclusion energy negative) in that case.

It is illustrated here that the embedded (with Si^{1-} ion and/or Si atom, to a lesser degree) $Si_{28}H_{28}$ fullerene prototype can be considered as an attractive alternative to the well-known reconstructed bulk nanocrystal model. Such a fullerene model(s) in addition could account (at least partly) for the weak emission at 2.8 eV, which has been correlated with a similar very weak peak in the calculated absorption spectra.[18] Moreover, under certain well stated conditions, as it will be shown bellow, even the traditional "bulk reconstructed" prototype (as well as other "bulk" prototypes discussed in the literature[19]) can be also obtained from the embedded fullerene model, in a simple and straightforward way (much easier compared to the standard prototype from the $Si_{29}H_{36}$ nanocrystal). Certainly, no matter how attractive or intriguing the present interpretation might be, the final criterion would be the comparison with experiment. To this end, the present theoretical results which are presented in Sec. II are compared in Sec. III to experiment, and to each other. The main conclusions of the present work are summarized in Sec. IV.

II. THEORETICAL RESULTS FOR THE STRUCTURAL AND ELECTRONIC CHARACTERISTICS

The results described here have been obtained within the framework of density-functional theory (DFT) and time-dependent DFT (TDDFT) using the B3LYP functional, following the methodology described in detail in Refs. 20 and 21, using spin polarized wave functions for the anionic clusters. This methodology has been shown (by comparison to high level *ab initio* methods and experimental data) to produce accurate structural, electronic, and optoelectronic data.[5,13–15]

The structural model shown in Figs. 1(a) and 1(a′) is a spherical piece of crystalline silicon containing 29 Si atoms and 36 terminal hydrogens. This was the first candidate in the search for a realistic structural prototype of the 1 nm luminous silicon nanostructure (see for instance page 49 of Ref. 19), since it is a well-known (from earlier studies of porous silicon and its constituents nanocrystals[4,5,13–15]) "bulklike" nanocrystal of about the right size (1 nm).[17–19]

The $Si_{29}H_{24}$ reconstructed prototype is shown in Figs. 1(b) and 1(b′), whereas the $Si_{29}H_{28}^{1-}$ embedded fullerene (as well as the isostructural neutral $Si_{29}H_{28}$ "fullerene") is shown in Figs. 1(c) and 1(c′). As we can see in these figures, the reconstructed prototype is clearly different from the $Si_{29}H_{28}^{1-}$ embedded fullerene, although it resembles somehow the D_{2d} $Si_{29}H_{24}$ structure obtained from the $Si_{24}H_{24}$ fullerene and a Si_5 central core, shown in Figs. 1(d) and 1(d′). This D_{2d} (near T_d) structure looks very much alike the $Si_{29}H_{24}^{Nano2}$ alternative prototype in Refs. 18 and 19.

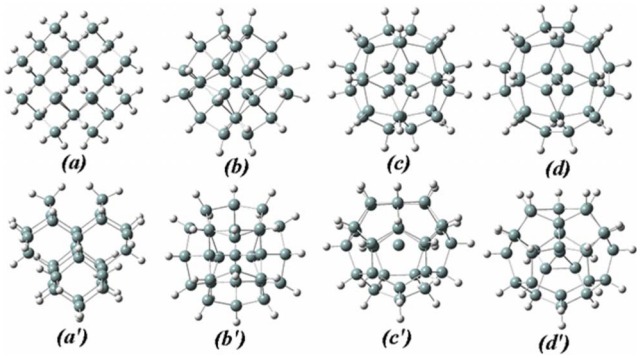

FIG. 1. (Color online) The key structural prototypes for the 1 nm ultrabright silicon nanoparticle shown in two different views (in top and bottom of the figure): [(a) and (a′)] $Si_{29}H_{36}$ bulklike; [(b) and (b′)] $Si_{29}H_{24}$ reconstructed; [(c) and (c′)] $Si_{29}H_{28}$ and $Si_{29}H_{28}^{1-}$ embedded fullerenes; and [(d) and (d′)] the $Si_5@Si_{24}H_{24}$ stuffed fullerene.

The prototypes in Figs. 1(b) and 1(c) are not only structurally different, but they also have different electronic properties, as can be seen in Fig. 2. The HOMO orbital of the $Si_{29}H_{28}^{1-}$ embedded fullerene structure of Fig. 1(c), contrary to the corresponding orbital of the reconstructed structure of Fig. 1(b), is fully localized in the central silicon atom (ion). Similarly, in the fullerene structure the spin density is also fully localized in the central atom. This could be very important (and very promising) for applications on quantum computing.[28] It is interesting to note at this point that in the corresponding neutral $Si_{29}H_{28}$ fullerene the HOMO orbital, as is shown in Fig. 2(g), is delocalized throughout the cluster, although the spin density in Fig. 2(k) is localized around the central atom inside the fullerene.

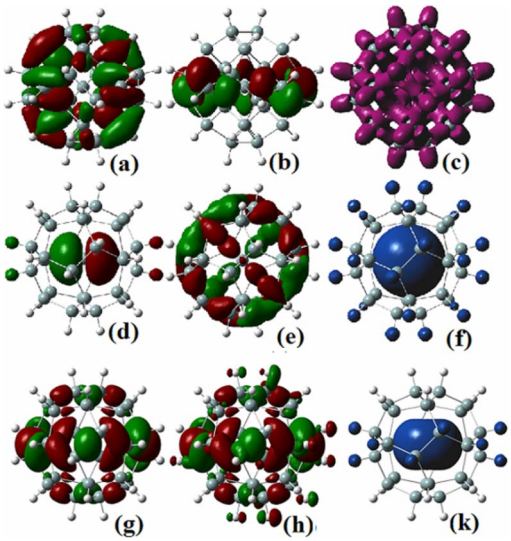

FIG. 2. (Color online) Comparison of the electronic properties between the reconstructed $Si_{29}H_{24}$ (top), embedded $Si_{29}H_{28}^{1-}$ (middle), and embedded $Si_{29}H_{28}$ (bottom) nanoparticles. HOMO orbitals are shown in (a), (d), and (g) and LUMO orbitals in (b), (e), and (h). The total electronic density of $Si_{29}H_{24}$ is shown in (c); whereas the spin density of $Si_{29}H_{28}^{1-}$ and $Si_{29}H_{28}$ are shown in (f) and (k), respectively.

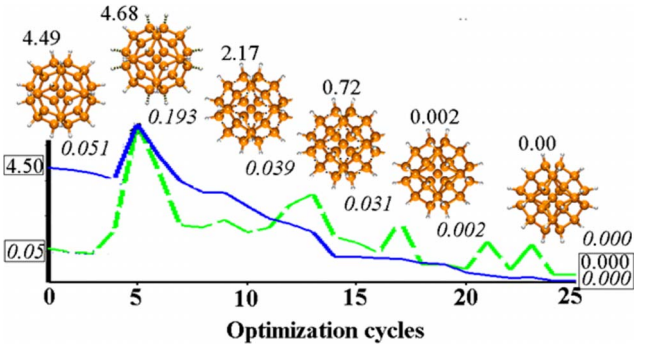

FIG. 3. (Color online) The route from the embedded $Si_{29}H_{28}^{1-}/Si_{29}H_{24}$ fullerene to the standard reconstructed $Si_{29}H_{24}$ prototype. The relative energy (blue solid line) and the absolute rms value of the gradient (proportional to the magnitude of the "force") in broken green line, are also given (the gradient in italics) for selective intermediate structures.

For the neutral embedded fullerene the HOMO and LUMO orbitals look very much alike. In all cases the LUMO orbitals are delocalized throughout the nanocluster. Looking closer to the HOMO orbital of the $Si_{29}H_{28}^{1-}$ embedded fullerene in Fig. 2(d) we can see that only four hydrogens (attached to four silicon atoms which are slightly closer to the central atom than the rest) out of a total of 28, participate in the formation of this orbital. If we eliminate these four particular hydrogens and consider the remaining neutral $Si_{29}H_{24}$ embedded fullerene, as we can see in Fig. 3, after geometry optimization we finally obtain the standard reconstructed bulk prototype. Apparently, this route (of eliminating four "targeted" hydrogens out of 28) for obtaining the reconstructed bulk prototype looks much simpler, more physically appealing, and more straightforward compared to the standard method (of eliminating 12 out of 36 hydrogens). As we can see in Fig. 3, during the geometry optimization process a small barrier of about 0.19 eV is encountered which is overcome by the optimization process itself. The corresponding transition state, at 4.68 eV above the reconstructed $Si_{29}H_{24}$ reference structure, is a structure with 12 (out of 24) very elongated Si–H bonds which facilitate the rearrangement of Si–H and Si–Si bonds and the redistribution of bond charges. The energy gain during this process (from the $Si_{29}H_{24}$ embedded fullerene to the $Si_{29}H_{24}$ reconstructed bulk nanocrystal) is about 4.5 eV. Similarly the energy gained by embedding $Si_{28}H_{28}$ with Si^{1-} anion, the embedding or inclusion energy, is 3.16 eV, the largest compared to other "nearby" fullerenes such as $Si_{20}H_{20}$, $Si_{24}H_{24}$, or $Si_{32}H_{32}$. This energy is obtained by comparing the $Si_{28}H_{28}$ neutral cage energy plus the energy of an isolated Si^{1-} anion with the total energy of the $Si_{28}H_{29}^{1-}$ embedded cage.

The embedding energy for neutral Si atom is much-much smaller, as could be expected from the fact that we have fully saturated structures, for which the already strong binding is not expected to benefit from the presence of single Si atom at the center of the cage, more than 4 Å away from the interior surface of the cage. Although the size of the cage allows such inclusion, the interaction with the cage silicons is limited due to the spherical symmetry, which limits polarization, and charge redistribution. The exohedral hydrogens are charged slightly negative and the surface silicons slightly positive (Mulliken charges about $+0.3e$), in agreement with the relative electronegativity of silicon and hydrogen. The central silicon although practically neutral, it can be slightly charged depending on the total charge distribution (Mulliken charge $=+0.05e$, in the case of $Si@Si_{28}H_{28}$). Thus the embedding energy of the neutral Si atom could be very small (0. 1 eV for $Si@Si_{24}H_{24}$) or even negative. Indeed, the neutral Si atom embedding energy of $Si@Si_{28}H_{28}$ is negative (-0.53 eV) which means that the Si atom at the center of $Si_{28}H_{28}$ fullerene is in fact under pressure. This could have significant influence on the optical properties and its equilibrium position, among others.

III. COMPARISONS BETWEEN THE STRUCTURES AND EXPERIMENT

A. Cohesive and energetic characteristics

One way to compare the relative stabilities of the structures in Fig. 1, which have different number of hydrogen atoms, is through the binding or atomization energies. However, such comparison could be misleading because the contribution of hydrogen to the binding is not the same for all structures. A better choice, which was very successful in comparing the stability of various partially hydrogenated carbon fullerenes[31] and hydrogenated silicon nanowires,[32] is the cohesive energy E_{coh} instead of the binding energy (BE). (For $Si_{29}H_{28}^{1-}$, or $Si^{1-}@Si_{28}H_{28}$ the atomization energy is calculated with respect to the $28Si_{atom}+28H_{atom}+1Si^{1-}$ reference energy). The cohesive energy, E_{coh}, which depends on the structure's size, is defined by the relation

$$E_{coh}=[BE(Si_{N_{Si}}H_{N_H})+\mu_H N_H]/N_{Si},$$

where $BE(Si_{N_{Si}}H_{N_H})$ is the binding (or atomization) energy of the $(Si_{N_{Si}}H_{N_H})$ structure. $N_{Si}=29$, $N_H=24,28,36$ are the numbers of Si and H atoms, respectively; and μ_H is the chemical potential of H, which is taken at a constant value. Doing so, we have effectively removed the energy contribution of all Si–H bonds in every system and essentially considered the binding energy of the "silicon skeleton." Alternatively we could have used the "formation energy" which involves the chemical potential of silicon, μ_{Si}, as an additional term without altering the relative energy separations and stability differences between the structures. Obviously, from the experimental point of view, the system would tend to attain the minimum of the free energy which is practically equivalent to the minimum formation energy, and therefore to the maximum cohesive energy. Indeed, similar calculations for $C_{60}H_{60}$ and partially hydrogenated $C_{60}H_n$ ($n=1,60$) cages and nanotubes[31] have shown that stable structures which have been synthesized experimentally correspond to the largest values of calculated cohesive energies.

The constant value of the chemical potential μ_H is evaluated ($\mu_H=-3.46$ eV) in such way that zero corresponds to the value at which the formation energy of silane (SiH_4) is zero. For similar or uniform systems, such as the (partially hydrogenated) fullerenes,[31] such a choice is very good. However, for the comparison of (drastically) different systems,

TABLE I. Binding (E_b) and cohesive energies (E_{coh}) together with HOMO-LUMO (E_{HL}) and optical (E_g) gaps in eV. For the last two structures (labeled as in Fig. 1) the embedding energy (E_{emb}) is also listed. E_{coh} has been evaluated using both, the constant value μ_H=−3.46 eV, (top line of the row), and the values of μ_H calculated separately for each structure (numbers in parenthesis, second line of the E_{coh} row).

	Structures				
E	$Si_{29}H_{36}$ 1(a)	$Si_{29}H_{24}$ 1(b)	$Si_{29}H_{24}$ 1(d)	[a]$Si_{29}H_{28}^{1-}$ 1(c)	$Si_{29}H_{28}$ 1(c)
E_b	6.98	5.84	5.81	6.26(8)	6.08
E_{coh}	2.69	2.97	2.94	2.92	2.74
	(3.07)	(2.92)		(3.16)	(3.13)
E_{emb}				3.15	−0.53
E_{HL}	5.1	3.9	3.6	2.3	3.4
E_g	4.5	3.3	3.2	2.7	2.6

[a]*The reference energy E_0 for the binding, cohesive and embedding energy of* $Si_{29}H_{28}^{1-}$ *is* $E_0=28E(Si_{atom})+28E(H_{atom})+1E(Si^{1-})$.

such as bulklike nanocrystals and doped fullerenes, the chemical potential μ_H should be evaluated (by adding and/or removing hydrogens) separately for each system. In such a process various positions for removal or addition of hydrogen should be examined to produced a (weighted, according to the number of equivalent positions) average value of μ_H. In the present work both methods have been used.

The cohesive energy E_{coh} together with the binding energy per silicon atom, $E_b=BE(Si_{N_{Si}}H_{N_H})/N_{Si}$, the HOMO-LUMO, E_{HL} and the optical absorption gap, E_g, are given in Table I for each one of the structures studied here. The HOMO-LUMO gap is also a zeroth order approximation of the chemical hardness of the structures. As we can see in Table I, for the first three bulklike structures the HOMO-LUMO gap scales rather well with the values of the binding energies, although it fails completely for the last two fullerenelike structures. On the basis of the binding energy the most stable structure is the unreconstructed bulk nanocrystal, followed by the two fullerene structures. The standard reconstructed model is only third in this comparison. Yet, as was mentioned before, this model was rejected on the basis of its optical spectrum (note the optical gap of 4.5 eV for this structure). Therefore, in full consistency with the earlier discussion on the significance of the cohesive (or of formation) energy, we are lead to declare the cohesive energy, E_{coh}, as the best criterion of stability for the candidate structures.

The results for the cohesive energy at the top line in the third row of Table I have been obtained using the constant value of the chemical potential μ_H=−3.46 eV. However, a better choice would have been the separate calculation of the chemical potential independently for each structure, taking into account the different nature of bonding and binding,. The results in the bottom line of the third row correspond to this choice. According to the first choice of the chemical potential the most stable structure is the standard reconstructed $Si_{29}H_{24}$ model with second the $Si_{29}H_{24}$ stuffed $Si_{24}H_{24}$ fullerene ($Si_5@Si_{24}H_{24}$), both originating, as we have shown earlier, from doping of the $Si_{28}H_{28}$ and $Si_{24}H_{24}$ fullerenes. However, on the basis of the second choice of chemical potential (bottom line of the third row in Table I) the most stable structure is the $Si_{29}H_{28}^{1-}$ (or $Si^{1-}@Si_{28}H_{28}$), with second the $Si_{29}H_{28}$ ($Si@Si_{28}H_{28}$) fullerene. Both of these models are consistent with the general observation that the source of the blue luminescence consists of two distinct structural units (one atomiclike and one fullerenelike). The small cohesive energy difference (0.03 eV per silicon atom) between the "top structures," which is similar to the energy difference using the first choice of the chemical potential could be easily overcome by the production conditions, although the embedding energy favors by far the $Si^{1-}@Si_{28}H_{28}$ fullerene. It becomes apparent that, in this complex and complicated situation, the experimental data (as many as possible) will be the decisive criterion in choosing the best prototype.

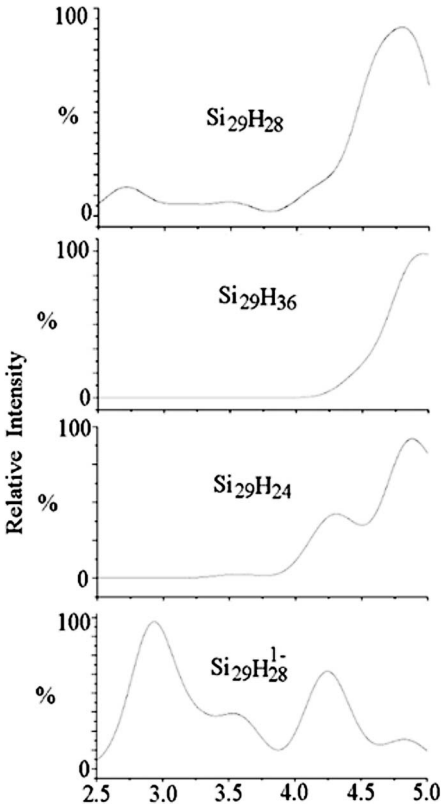

FIG. 4. The calculated absorption spectra for the four key structural prototypes. From top to bottom are shown the spectra of $Si_{29}H_{28}$ (neutral), $Si_{29}H_{36}$ unreconstructed crystalline, $Si_{29}H_{24}$ reconstructed bulklike, and $Si_{29}H_{28}^{1-}$ fullerene.

B. Comparison of the absorption spectra

The most critical and important experimental test is the optical (absorption and/or emission) spectrum. On the basis of this spectrum the "fully crystalline" unreconstructed prototype of Fig. 1(a) was rejected. This can be also seen from the absorption edges (optical gaps, E_g) in the last row of Table I. In Fig. 4 we compare the calculated absorption spec-

tra for the four (two bulklike and two fullerenelike) key structures.

These spectra were obtained by the TDDFT method using the B3LYP hybrid functional. It has been illustrated[5,13–15] that this particular method gives very accurate results comparable to high level *ab initio* multireference calculations. For the results in Fig. 4 a Gaussian broadening of 0.14 eV was used, which qualitatively represents the temperature and size averaging appropriate for this system.[18,19] This also allows direct comparison with the results presented in Refs. 18 and 19 (see for instance page 51 of Ref. 19), using the same broadening.

The $Si_{29}H_{24}$ surface-reconstructed bulklike structure could be considered as the reference structure, since its calculated spectrum (third from the top in Fig. 4) was found in reasonable agreement with experiment, although it does not fully reproduce the experimental measurements, and in particular the observed[18] emission peak at 2.8 eV.

This emission peak was initially associated with an extremely weak (1/1000) absorption peak at about the same energy observed in the calculated absorption spectrum[18] near the HOMO-LUMO edge at about 2.5 eV according to the calculations of Rao *et al.*,[18] although the Stokes shift was estimated at about 0.5 eV (0.4 eV according to the quantum Monte Carlo results[17]). Nevertheless, it is a common practice in many calculations[4–7] to use the excitation spectrum, corresponding to absorption at the ground-state geometry in order to interpret the emission spectrum, the two loosely assumed to be roughly "similar," besides a "small" almost uniform shift (the Stokes shift, i.e., the difference between absorbed and emitted photon energies). On top of this, the excitation spectrum can be calculated more easily and accurately within the time-dependent density-functional theory. The emission spectra could be approximately estimated by relaxing the structure in the excited state (excited state optimization). The use of the B3LYP functional in this case is believed (at least by the present author) to be essential. It should be mentioned that the present calculation (based on TDDFT/B3LYP) for the reconstructed nanoparticle yields a very weak absorption peak corresponding to the absorption edge at 3.3 (see Table I), which considering the Stokes shift around 0.5 eV could in principle account for the 2.8 eV emission. The same is true for the $Si_5@Si_{24}H_{24}$ fullerene shown in Figs. 1(d) and 1(d′), with an absorption edge at 3.2 eV, and the two embedded fullerene models which are characterized by much stronger absorption peaks in the region of 3.2–3.5 eV. Yet, since it is not clear whether or not these peaks are directly related with the emission lines in the region of 2.8 eV; and since we are mainly interested in comparison between the structures, all comparisons will be made here with respect to the calculated excitation (absorption) spectrum, unless otherwise is stated. After all, the 2.8 eV emission is not the central point of this paper.

As we can see in Fig. 4, instead of the extremely weak absorption peak of Ref. 18, we have a very strong peak (the "missing" peak?) in the $Si_{29}H_{28}$ neutral Si-atom embedded fullerene, perhaps a bit exaggerated in strength. A similar peak is present with much larger relative intensity in the $Si_{29}H_{28}^{1-}$ embedded fullerene. As a matter of fact in this case it corresponds to the maximum intensity in this energy (wavelength) region, which looks obviously incompatible with the well-known experimental results.

One could attempt to attribute the exaggerated relative intensities to an artifact of the broadening process, or even of the method of calculation regarding the intensities (oscillator strengths) which obviously carry larger uncertainties compared to the excitation energies. This last possibility, however, can be readily ruled out in view of the well tested (in comparison to both, very high level *ab initio* methods, and experiment) performance of this method in several similar cases.[5,13–15,21]

Yet, considering the overall good agreement of the remaining major peaks and taking also into account the cohesive criterion one might suspect and suggest other possibilities for the 2.8 eV peak. One such possibility is resonant absorption by oxygen impurities of this peak, which was really there originally, so that its intensity is drastically diminishing in the experimental observations.

As has been illustrated by this author and collaborators,[14,15] "oxygen impurities" through the Si=O bond can give relatively strong peaks in this energy region. Rao *et al.*[18] have also suggested (in a different respect) that the possible origin of this peak is related to oxygen impurities. Therefore, if everything else is consistent this could be a strong possibility.

On the other extreme, if one strictly sticks to the reconstructed prototype for whichever reasons, then the route of formation (the formation path) shown in Fig. 3, which in the author's opinion is realistic beyond any reasonable doubt, provides an alternative suggestion for the 2.8 eV peak. In this case, the 2.8 eV emission peak could be due to one intermediate metastable state, such as the one obtained at the sixth optimization cycle in Fig. 3. Indeed the HOMO-LUMO (Kohn-Sham) gap of the structures around the saddle point in Fig. 3 ranges between 2.4 and 3.1 eV, which is highly suggestive of a corresponding emission peak at around 2.8 eV.

The final suggestion, which is a combination of the two extremes (and as such could appear to be more attractive) is that the reconstructed and fullerene structures coexist, providing a spectrum which is in reality a (weighted) average of the two (or three?). By examining and comparing additional properties and characteristics, one might be able to draw more definite conclusions.

C. Comparison of vibrational and electrostatic properties

One obvious property to consider is the vibrational, and in particular the infrared (IR) spectrum of the three candidate structures. This spectrum, as well as the Raman spectrum for all three structures is dominated by the very intense (peak intensity) Si–H stretching mode at around 2150 cm^{-1}, which hides the remaining modes (if drawn in the same scale). This is particularly true for the Raman spectrum. Therefore instead of drawing the IR or Raman spectra, we provide a list of IR frequencies and relative intensities (for frequencies with relative intensities larger than 1%), together with the dominant (highest intensity) Raman frequency, in Table II.

As we can see in this table, the largest difference in frequency between the three structures is around 1.6% (or about

TABLE II. Comparison of the dominant IR vibrational frequencies (all of t_2 symmetry) and the peak intensity Raman frequency (underlined), of a_1 symmetry, in cm^{-1}. The static polarizabilities, in atomic units (a.u.), are listed in the last row.

	Structures		
Frequencies	$Si_{29}H_{24}$ 1(b)	$Si_{29}H_{28}$ 1(c)	$Si_{29}H_{28}^{1-}$ 1(c)
	654 (9)	690 (10)	696 (7)
	675 (19)	702 (14)	708 (10)
	725 (20)	714 (47)	721 (29)
	2153 (4)	2162 (3)	2124 (8)
	2162 (1)	2168 (20)	2131 (38)
	2167 (100)	2174 (100)	2138 (100)
	2174 (a_1)		2152 (a_1)
Polarizabilities	813.2	822.2	964.5

35 cm^{-1} for the dominant Si–H stretching mode), which is practically at the edge of the accuracy of the calculations. The accuracy of the intensities is even lower. Therefore, it seems difficult to decide on the basis of the IR frequency spectrum alone which structure corresponds to the experimental spectrum.[19] The same is true (to the same or even larger extent) for the Raman spectrum, which for both species is fully dominated from the very narrow region around the peak Raman intensity, given in Table II. For both $Si_{29}H_{24}$ and $Si_{29}H_{28}^{1-}$ besides the region of peak intensity (which is practically the same for IR and Raman), the only other region with relative intensity (activity) larger than 1% is the region of the first breathing mode, at 238 cm^{-1} for the reconstructed or 225 cm^{-1} for $Si_{29}H_{28}^{1-}$ with relative intensities around 4%. The spectra look pretty much the same.

The vibration of the central Si ion in $Si_{29}H_{28}^{1-}$ corresponds to a soft threefold degenerate t_2 mode with frequency $\approx$80 cm^{-1} and relative intensity around 0.4%. The associated force constant is only 0.1 mDyne/Å, compared to values around 2.8–2.9 mDyne/Å for the higher intensity high frequency modes. This is an additional illustration of the extremely weak coupling of the central Si ion with the rest.

In Table II we also list the calculated polarizability, which is a uniquely defined property for each structure. These values have been obtained at the correlated TDDFT /B3LYP level of theory using the triple-ζ valence polarized (TZVP) basis set. As would be expected the polarizability of the $Si_{29}H_{28}^{1-}$ embedded fullerene is the largest, in full agreement with the distribution of atomic charges for each cluster shown in Fig. 5. The value of polarizability calculated in Ref. 19 (page 54) for the standard reconstructed prototype is about 793 a.u., much less compared to the value obtained here at the TDDFT/B3LYP level of theory (813 a.u.). Apparently the difference is due to the different methods of calculation used in the two approaches. The polarizabilities of the neutral embedded fullerene and the bulk reconstructed prototypes are very close to each other. Therefore these two structures, contrary to $Si_{29}H_{28}^{1}$, cannot be "distinguished" on the basis of polarizability measurements.

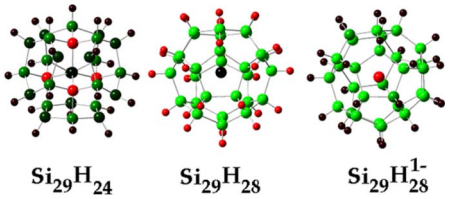

FIG. 5. (Color online) The distribution of atomic charges for each structure, obtained by Mulliken population analysis. Red color (online) indicates negative charge and green positive charge. Black color specifies roughly neutral (or very small positive, as in the case of $Si_{29}H_{28}$, or very small negative) charge.

D. Comparison of the NMR chemical shifts

A different property which would be useful to compare is the NMR chemical shifts, which are usually evaluated and measured relative to the corresponding chemical shifts in TMS. The calculated (relative to TMS) chemical shifts of hydrogen for the three key structures are listed in Table III. These values, which have been obtained at the Hartree-Fock (HF) level of theory, are only indicative. They could be certainly improved by changing the level of theory and basis sets, if needed. However, for relative comparisons they are quite adequate, especially if we take as a reference point the results for the reconstructed prototype. Nayfeh in Ref. 19 (see in particular page 19) refers to a nanoprobe H NMR study of fresh prepared particle's dispersion in d-THF. In this study the spectrum exhibits a strong signal of Si–H groups (2.5–2.6 ppm), although it contains other peaks (around 0.1, 0.9, and 1.2–1.4 ppm) attributed to a hydrocarbon contamination.

According to the results of Table III, we would expect two close-lying ($\Delta\delta \approx 1$ ppm) lines of equal strength, which, due to the limited resolution, could appear as one line. However, with this reasoning the $Si_{29}H_{28}^{1-}$ fullerene would be equally acceptable. This is not quite true for the neutral $Si_{29}H_{28}$ fullerene. A clear distinction between the two close-behaving species could be perhaps accomplished by considering also the silicon chemical shifts.

To accommodate the characterization, we compare in Fig. 6 the Si chemical shifts. It becomes clear from Fig. 6 that such results could in principle distinguish between the two "dominant" species independently of the feasibility of the corresponding measurements. The present author is not aware of such measurements up to now.

TABLE III. Comparison of the NMR chemical shifts of H (δ) relative to TMS, in ppm.

	Structures		
δ	$Si_{29}H_{24}$ 1(b)	$Si_{29}H_{28}$ 1(c)	$Si_{29}H_{28}^{1-}$ 1(c)
	3.2 (12)	2.5 (4)	3.3 (12)
	4.1 (12)	3.1 (8)	3.5 (12)
		4.0 (8)	3.8 (4)
		4.2 (8)	

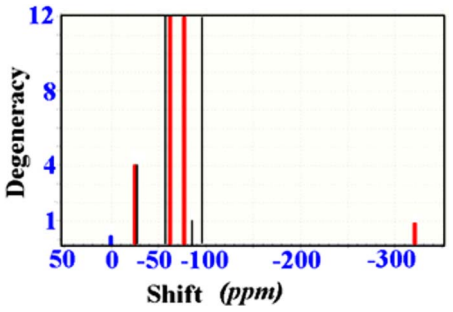

FIG. 6. (Color online) The relative to TMS NMR chemical shifts of silicon for distribution of atomic charges for $Si_{29}H_{24}$, with thin black lines, and $Si_{29}H_{28}^{1-}$, in thick red (online) lines.

It is interesting to observe in Fig. 6 that although the chemical environment of the central atoms (lines with degeneracy equal to 1) is drastically different in the two structures, the chemical environment of the four "nearest neighbors" of the central atoms (lines with degeneracy equal to 4) are not that much different.

IV. CONCLUSIONS

A different approach and some alternative prototypes based on silicon fullerenes have been presented and compared with the standard bulklike reconstructed prototype for the luminous 1 nm silicon nanoparticle. The strongest candidate is the $Si_{29}H_{28}^{1-}$ (or better the $Si^{1-}@Si_{28}H_{28}$) fullerene in which the extra charge and the excess spin are fully localized in the central atom (anion), which is only weakly coupled to the rest surface atoms. This is physically appealing, and technologically very attractive for novel applications, for instance, in quantum computing. The high stability of this fullerene, according to the results of Table I, should be related to the closure of the α-t_{1u} subshell (HOMO orbital). This system, regardless of its direct or indirect relationship and association with the 1 nm luminous nanoparticle, is very interesting and very promising in itself.

Perhaps one could be skeptical about the direct association of $Si^{1-}@Si_{28}H_{28}$ with the 1 nm luminous nanoparticle, in particular concerning the absorption spectrum in Fig. 4 (although, alternative interpretations have been suggested). It is important to stress that neither the standard reconstructed prototype accounts fully for the observed spectrum due to the same 2.8 eV peak which has no absorption counterpart in the calculated excitation spectrum (as shown in Fig. 4) although it has been detected experimentally. The excitation spectrum of $Si_{29}H_{28}^{1-}$ fullerene, on the other hand is characterized by such a peak but the magnitude of its intensity is unrealistic (unless there are other agents with resonant absorption in this region of photon energy. Rao *et al.*[18] have attributed this peak to possible oxygen contamination or other defects. Indeed, our earlier calculations[14] have clearly associated this peak with absorption through the Si=O double bonds. Therefore, the possibility of absorption of an initially strong peak by oxygen is not totally unfounded. This remains to be seen by additional experiments.

Needless to say that the existing IR, Raman, and proton NMR data cannot clearly distinguish between the two models ($Si_{29}H_{28}^{1-}$ fullerene and $Si_{29}H_{24}$ reconstructed bulklike) within the experimental and calculational uncertainties.

Independently of the validity and acceptance of the direct association of the $Si_{29}H_{28}^{1-}$ fullerene with the 1 nm luminous nanoparticle described above, the indirect association through the interpretation of Fig. 3 is fully valid. This fullerene provides, at worst, a well defined transparent route for the production of the standard reconstructed prototype. Apparently this route (through the elimination of four well defined, "targeted" hydrogens) is more straightforward and attractive compared to the elimination (and reconstruction) of 12 hydrogens from the bulk $Si_{29}H_{36}$ nanocrystal.

Finally, it is interested to observe that the next bright nanoparticle at about 2.6 nm which corresponds to a "magic" T_d bulk nanocrystal, also corresponds (in size and symmetry) to the embedded $Si_{77}H_{76}^{1-}$ fullerene of T_d symmetry. This could perhaps be indicative of a more general trend or a deeper interpretation. It is the strong conviction of the present author that the real and final solution to the problem of the real structure of the 1 nm luminous nanoparticle would be within the embedded (by Si^{1-} or Si) fullerene framework. This (together with several open questions) remains to be seen.

The present results, which could have a strong impact not only on silicon nanoparticles but also on fullerene-structured silicon nanowires,[33] should be considered as a stimulus for additional and more accurate work on this field, both experimental and theoretical.

[1] L. T. Canham, Appl. Phys. Lett. **57**, 1046 (1990).
[2] J. P. Wilcoxon, G. A. Samara, and P. N. Provencio, Phys. Rev. B **60**, 2704 (1999).
[3] M. V. Wolkin, J. Jorne, P. M. Fauchet, G. Allan, and C. Delerue, Phys. Rev. Lett. **82**, 197 (1999).
[4] S. Schuppler, S. L. Friedman, M. A. Marcus, D. L. Adler, Y. H. Xie, F. M. Ross, Y. L. Cha-bal, T. D. Harris, L. E. Brus, W. L. Brown, E. E. Chaban, P. F. Szajowski, S. B. Christman, and P. H. Citrin, Phys Rev. Lett. **72**, 2648 (1994); Phys. Rev. B **52**, 4910 (1995).
[5] C. S. Garoufalis, A. D. Zdetsis, and S. Grimme, Phys. Rev. Lett. **87**, 276402 (2001).
[6] E. Degoli, G. Cantele, E. Luppi, R. Magri, D. Ninno, O. Bisi, and S. Ossicini, Phys. Rev. B **69**, 155411 (2004).
[7] I. Vasiliev, J. R. Chelikowsky, and R. M. Martin, Phys. Rev. B **65**, 121302 (2002).
[8] A. Puzder, A. J. Williamson, J. C. Grossman, and G. Galli, J. Am. Chem. Soc. **125**, 2786 (2003).
[9] A. Puzder, A. J. Williamson, J. C. Grossman, and G. Galli, J. Chem. Phys. **117**, 6721 (2002).

[10] Z. Zhou, L. Brus, and R. Friesner, Nano Lett. **3**, 163 (2003).
[11] M. Luppi and S. Ossicini, J. Appl. Phys. **94**, 2130 (2003).
[12] Z. Zhou, R. A. Friesner, and L. Brus, J. Am. Chem. Soc. **125**, 15599 (2003).
[13] A. D. Zdetsis, C. S. Garoufalis, and S. Grimme, in *Quantum Dots: Fundamentals, Applications, and Frontiers (Crete 2003)*, edited by B. A. Joyce *et al.*, NATO Science Series, Vol. 190 Series II, Mathematics, Physics, and Chemistry (Kluwer-Springer, Dordrecht, The Netherlands, 2005), pp 317-332.
[14] C. S. Garoufalis and A. D. Zdetsis, Phys. Chem. Chem. Phys. **8**, 808 (2006); J. Phys.: Conf. Ser. **10**, 69 (2005).
[15] A. D. Zdetsis, Rev. Adv. Mater. Sci. **11**, 56 (2006).
[16] O. Akcakir, J. Therrien, G. Belomoin, N. Barry, J. D. Muller, E. Gratton, and M. Nayfeh, Appl. Phys. Lett. **76**, 1857 (2000).
[17] L. Mitas, J. Therrien, R. Twesten, G. Belomoin, and M. Nayfeh, Appl. Phys. Lett. **78**, 1918 (2001).
[18] S. Rao, J. Sutin, R. Clegg, E. Gratton, M. H. Nayfeh, S. Habbal, A. Tsolakidis, and R. M. Martin, Phys. Rev. B **69**, 205319 (2004); A. Tsolakidis and R. M. Martin, *ibid.* **71**, 125319 (2005).
[19] M. Nayfeh and L. Mitas, in *Nanosilicon*, edited by V. Kumar (Elsevier, Amsterdam, 2007).
[20] A. D. Zdetsis, Phys. Rev. B **75**, 085409 (2007).
[21] A. D. Zdetsis, Phys. Rev. B **76**, 075402 (2007).
[22] V. Kumar and Y. Kawazoe, Phys. Rev. B **75**, 155425 (2007).
[23] V. Kumar and Y. Kawazoe, Phys. Rev. Lett. **90**, 055502 (2003).
[24] A. J. Karttunen, M. Linnolahti, and T. A. Pakkanen, J. Phys. Chem. C **111**, 2545 (2007).
[25] Z. Chen, H. Jiao, D. Moran, A. Hirsch, W. Thiel, and P. v. R. Schleyer, J. Phys. Chem. A **107**, 2075 (2003).
[26] D. Moran, F. Stahl, E. D. Jemmis, H. F. Schaefer, and P. v. R. Schleyer, J. Phys. Chem. A **106**, 5144 (2002).
[27] A. D. Zdetsis, in *Stability of Materials*, edited by A. Gonis, P. E. A. Turchi, and J. Kudrnovsky, NATO Advanced Studies Institute Series B: Physics (Plenum Press, New York, 1996), Vol. 355, p. 455.
[28] W. Harneit, M. Waiblinger, C. Meyer, K. Lips, and A. Weidinger, in *Fullerenes for the New Millennium*, edited by K. M. Kadish, P. V. Kamat, and D. Guldi (The Electrochemical Society, Pennington, USA, 2001); S. Park, D. Srivastava, and K. J. Cho, J. Nanosci. Nanotechnol. **1**, 75 (2001); W. Harneit, Phys. Rev. A **65**, 032322 (2002).
[29] M. N. Nayfeh, S. R. Habbal, and S. Rao, Astrophys. J. Lett. **621**, L121 (2005).
[30] A. Webster, Nature (London) **352**, 412 (1991).
[31] A. D. Zdetsis, Phys. Rev. B **77**, 115402 (2008).
[32] A. D. Zdetsis, E. N. Koukaras, and C. S. Garoufalis, Appl. Phys. Lett. **91**, 203112 (2007).
[33] B. Marsen and K. Sattler, Phys. Rev. B **60**, 11593 (1999).